International Journal of Hydrogen Energy 125 (2025) 37–47

Contents lists available at ScienceDirect

International Journal of Hydrogen Energy

journal homepage: www.elsevier.com/locate/he

Strain engineering of $LiFePO_4$ cathodes: Effects on voltage, energy density, and electronic structure for lithium-ion batteries

Abdelmajid Assila [a,*], Ikram Belkoufa [a], Seddiq Sebbahi [a,b], Amine Alaoui-Belghiti [a], Said laasri [a,**], El-kebir Hlil [c], Mouhaydine Tlemçani [d,e], Abdelowahed Hajjaji [a]

[a] Chouaib Doukkali University of El Jadida, National School of Applied Sciences, Energy Science Engineering Lab, El Jadida, Morocco
[b] Research Institute for Solar Energy and New Energies (IRESEN), Morocco
[c] Univ. Grenoble Alpes, CNRS, Grenoble INP, Institut N'eel, 38000, Grenoble, France
[d] Department of Mechatronics Engineering, School of Science and Technology, Universidade de Evora, Colégio Luis Antonio Verney, Rua Romao Ramalho, N° 59, 7000–671, Evora, Portugal
[e] Instrumentation and Control Laboratory, Institute of Earth Sciences, Universidade de Evora, Colégio Luis Antonio Verney, Rua Romao Ramalho, N° 59, 7000–671, Evora, Portugal

ARTICLE INFO

Handling Editor: Suleyman I. Allakhverdiev

Keywords:
Strain engineering
Batteries
$LiFePO_4$
OCV
Energy density

ABSTRACT

Improving cathodes in commercial battery applications is one of the current trends aimed at achieving optimal performance for energy storage and reuse. In this study, triaxial tensile/compressive strains were applied to $LiFePO_4$ and $FePO_4$ structures, which are the main components of the cathode in lithium batteries. The goal is to control the open-circuit voltage (OCV) and energy density (E_d) under the influence of these strains, as well as to study the structural, electronic, and electrochemical properties. The study is based on density functional theory (DFT) and uses the generalized gradient approximation (GGA) developed by Perdew-Wang 1991 (PW91). The results show that the voltage of the undeformed systems is 3.92 V, and the energy density is 666.83 Wh/kg for the undeformed systems. Under a maximum tensile strain of $\varepsilon = +6$ % applied to $LiFePO_4$, the voltage decreases to 3.32 V, and the energy density drops to 564.42 Wh/kg. In contrast, for $FePO_4$, subjected to the same strain, the voltage decreases to 2.99 V and the energy density to 507.71 Wh/kg. When the $LiFePO_4$ system is subjected to a maximum compressive strain of $\varepsilon = -6$ %, the voltage and energy density decrease to 3.08 V and 523.28 Wh/kg, respectively. Similarly, when these strains are applied to $FePO_4$, the voltage drops to 2.82 V and the energy density to 478.46 Wh/kg. On the other hand, the interatomic distance of the studied features, as well as the volume and electronic charge density, vary depending on the intensity of the applied strains. The analysis of the total density of states showed that the characteristics of $LiFePO_4$ and $FePO_4$, in the absence of strain, behave as semiconductors, with a band gap of 2.265 eV and 1.831 eV, respectively. However, these characteristics undergo modifications under the effect of the applied strains.

1. Introduction

The world today is not the same as it was before the scientific revolution. Before this revolution, societies primarily met their energy needs by using the available natural resources [1,2]. At that time, access to energy was not a major concern for development [3]. This situation was partly due to a smaller population. However, after the scientific revolution and with advancements in the medical field, the population began to grow almost uncontrollably [4–6]. This rapid demographic increase led to a simultaneous rise in energy demand, as the improvement of living standards became an essential factor in this dynamic [7–9]. Thus, the relationship between population growth and increasing energy needs became increasingly critical in the context of our modern society [4]. Energy demand can be addressed from the production side, where innovative and sustainable solutions can be implemented [10–13]. However, a major challenge remains storing the produced energy and reusing it during peak demand periods [7]. To address this issue, it is essential to develop efficient energy storage technologies, such as lithium-based batteries $LiFePO_4$ or sodium-based batteries $NaFePO_4$, gravity-based energy storage systems, or hydrogen

* Corresponding author.
** Corresponding author.
E-mail addresses: assila.a@ucd.ac.ma (A. Assila), laasrisaid@yahoo.fr (S. laasri).

https://doi.org/10.1016/j.ijhydene.2025.04.075
Received 8 January 2025; Received in revised form 3 April 2025; Accepted 4 April 2025
Available online 10 April 2025
0360-3199/

storage [14–24]. These solutions will not only allow energy to be stored when production exceeds consumption but also enable its optimal use when energy needs are higher [25–29]. Thus, overcoming this storage challenge is crucial to ensuring a reliable and sustainable long-term energy supply [30,31]. For example, hydrogen can be stored in various forms, It can exist as a liquid in cryogenic tanks, as a gas in high-pressure tanks, or as a solid under well-defined conditions, particularly with a decomposition temperature that does not exceed a range of 289–393 K [18,32–35]. Moreover, the storage capacity should be greater than 6 % [36,37].

Another type of energy storage involves the use of lithium-ion batteries, such as $LiFePO_4$, or sodium-ion batteries, such as $NaFePO_4$ [22,38–44]. These batteries are particularly interesting due to their long lifespan [45–50]. For example, Zixuan Zhou and al. demonstrated that lithium-ion batteries based on $LiFePO_4$ can maintain a capacity of 96.30 % after 1500 cycles at 2 °C [51], 97.4 % after 100 cycles, and 95.2 % at 20 °C and 80.5 % at 40 °C after 2000 cycles [52], 80.6 % at 10 °C after 1500 cycles [41]. The total lithium extraction from the material could still reach 80.18 % of that from the brand-new electrode [26]. The $LiFePO_4$ possesses a theoretical specific capacity of ~170 mAh g^{-1}, thereby contributing to its relatively considerable energy density of ~544 Wh kg^{-1} [53–56]. These density and capacity characteristics make them a significant choice for many industrial applications, particularly in the electric vehicle sector and energy storage systems [25,57–59]. Moreover, $LiFePO_4$ batteries stand out for their safety and thermal stability under various applications, offering an extended lifespan for this type of vehicle and enhanced resistance to extreme conditions [60–64]. This makes them particularly well-suited for demanding uses [65,66].

In light of these numerous advantages, $LiFePO_4$ lithium batteries can be considered an important means for electrical energy storage and easy reuse [67–75]. However, a challenge remains: improving the cathode voltage, which should not exceed 4.5 V to avoid the risk of explosion and should not drop below 2.5 V to prevent irreversible reactions [65]. Indeed, several studies have addressed this issue using different methods. For example, Shucheng Wang and al. investigated the enhancement of the open-circuit voltage (OCV) by co-substituting Li with Mn and N, They observed that the OCV decreased from 3.43 V for the unsubstituted $LiFePO_4$ system to 3.19 V for the Mn and N co-substituted system [76]. On the other hand, Chandrani Nayak and al. performed substitution and co-substitution with Mn and Ni and found that the voltage could vary depending on the percentages of substitutions used [77]. Mourad Rkhis and al. improved the OCV by applying biaxial strains to $LiFePO_4$, They observed that it is possible to control the OCV, and that its value remains close to 3.78 V [65].

In this work, triaxial strains were applied to $LiFePO_4$ and $FePO_4$ systems to improve and control their effect on the energy absorption of lithium ions during the charge and discharge phases of lithium-ion batteries, as well as on the open-circuit voltage (OCV) and the energy density that the batteries can deliver. Additionally, the study also analyzed the effect of these strains on the electronic charge density and their influence on the structural properties of the materials. To our knowledge, no published work in the literature has addressed the development of these characteristics under triaxial strains. Only Mourad Rkhis and al, has applied biaxial strains, but solely to develop the OCV and energy density, while Zhang and al, and Lee and al, studied the improvement of the activation energy of Li^+ ions [58,65,74]. We believe that the method of applying triaxial strains could become a means of optimization and development for the cathodes of $LiFePO_4$ lithium-ion batteries, guiding future research toward the advancement of these cathodes.

2. Computational details

The calculations performed in this work were carried out using density functional theory (DFT), employing the Cambridge Serial Total Energy Package (CASTEP) computational code [78]. The exchange-correlation function was treated using the generalized gradient approximation (GGA), as adapted by Perdew-Wang 1991 (PW91) [79]. The valence electrons, whether originating from $LiFePO_4$ or $FePO_4$, were studied using ultrasoft pseudopotentials to ensure better optimization [80]. On the other hand, the treatment of electron correlation for the elements Li (2s), Fe (3d), P (3p), and O (2p) was done by applying the Hubbard correction using the (DFT + U) method [10,22]. The cutoff kinetic energy is 380 eV, and K-point set 1 × 2 × 3 for a minimization with a maximum force of 0.01 eV/Å, a maximum displacement of 5×10^{-4} Å, and a maximum stress of 0.02 GPa, and Self-Consistent Field (SCF) of 5×10^{-7} eV/atom for an energy of 5×10^{-6} eV/atom. The algorithm used is the Broyden–-Fletcher–Goldfarb–Shanno (BFGS) method [81,82]. After optimizing the structures of $LiFePO_4$ and $FePO_4$, we will subject them to triaxial strains ε_{xx}, ε_{yy}, and ε_{zz} (Fig. 1), both in tension and compression [18,83]. These strains will be applied along the [111] direction, that is, along the Ox, Oy, and Oz axes. This will allow the deformation of the lattice parameters a, b, and c, which will be subjected to strains ranging from $\varepsilon = 0$ % to $\varepsilon = +6$ % in tension, and from $\varepsilon = 0$ % to $\varepsilon = -6$ % in compression, with a step size of $\varepsilon = \pm 1$ % relative to the equilibrium parameters a_0, b_0, and c_0 of the $LiFePO_4$ and $FePO_4$ systems [84,85]. The following equation will model the strains:

$$\varepsilon_{xx} = \frac{a - a_0}{a_0} \times 100 \quad (1)$$

$$\varepsilon_{yy} = \frac{b - b_0}{b_0} \times 100 \quad (2)$$

$$\varepsilon_{zz} = \frac{c - c_0}{c_0} \times 100 \quad (3)$$

3. Results and discussion

3.1. Structural properties

Before examining the effect of triaxial strains on the open-circuit voltage and the structural and thermodynamic properties, we first carried out a structural optimization of the $LiFePO_4$ structure in the P_{nma} space group (N° 62) [76,77,86–88]. This system consists of 4 lithium, iron, and phosphorus atoms, as well as 16 oxygen atoms, which are arranged in a conventional unit cell. The optimization of this system allowed for the analysis of the interactions between these atoms and the determination of the unit cell parameters. The results of this optimization revealed the following values for the unit cell parameters: a = 10.42 Å, b = 6.06 Å and c = 4.73 Å with angles α = β = γ = 90°. These results are consistent with previous studies in the literature. This agreement highlights the validity of the optimization method used and suggests that the system shares similar characteristics with those previously observed: a = 10.34 Å, b = 6.03 Å and c = 4.73 Å, with α = β = γ = 90° [76], a = 10.34 Å, b = 6.01 Å and c = 4.70 Å with α = β = γ = 90° [89], and a = 10.29 Å, b = 6.05 Å and c = 4.68 Å, with α = β = γ = 90° [76], a = 10.349 Å, b = 6.031 Å and c = 4.722 Å, with α = β = γ = 90° [10].

3.2. The volume

The second parameter to study before applying triaxial strains to the $LiFePO_4$ and $FePO_4$ systems is the volume. This parameter is crucial for understanding how these two systems respond to the applied strains [22,65,76]. By analyzing the volume, it is possible to assess how the atoms interact and reorganize under triaxial strains, which can influence their thermodynamic and structural properties [84,85]. This understanding is essential for anticipating the behavior of the materials under real-world operating conditions. The results of the variation in volume for $LiFePO_4$ and $FePO_4$ under triaxial strains are shown in Fig. 2.

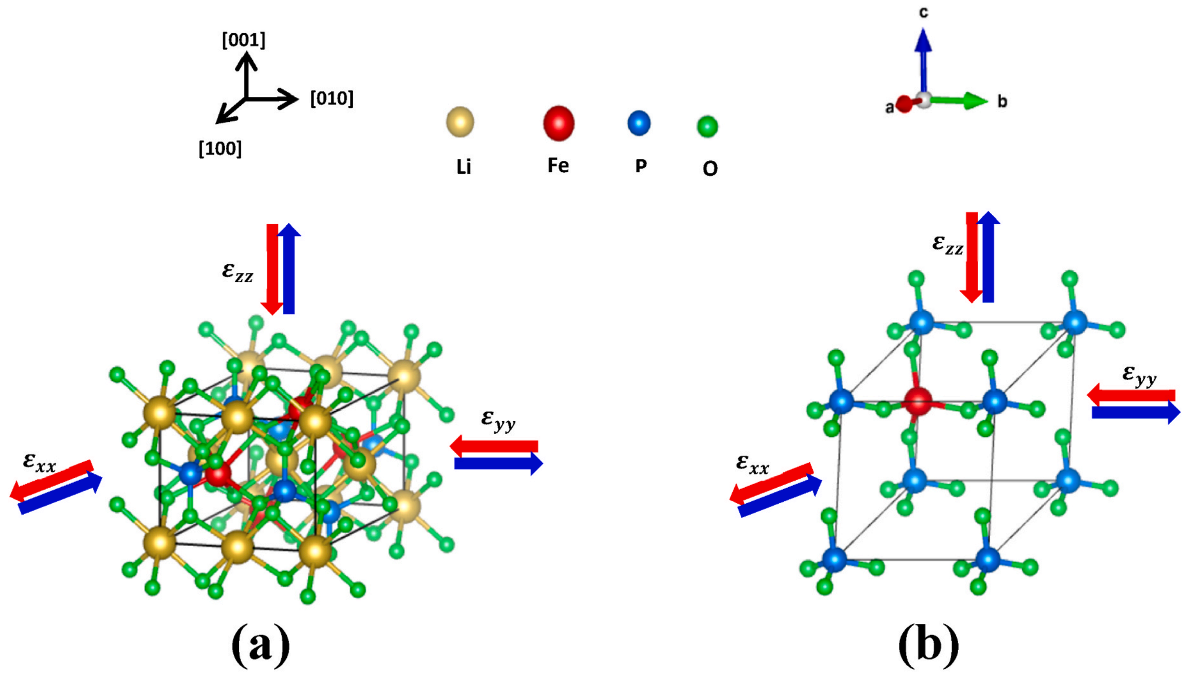

Fig. 1. Schematic representation of the triaxial tensile/compressive strains applied to $LiFePO_4$ (a) and $FePO_4$ (b).

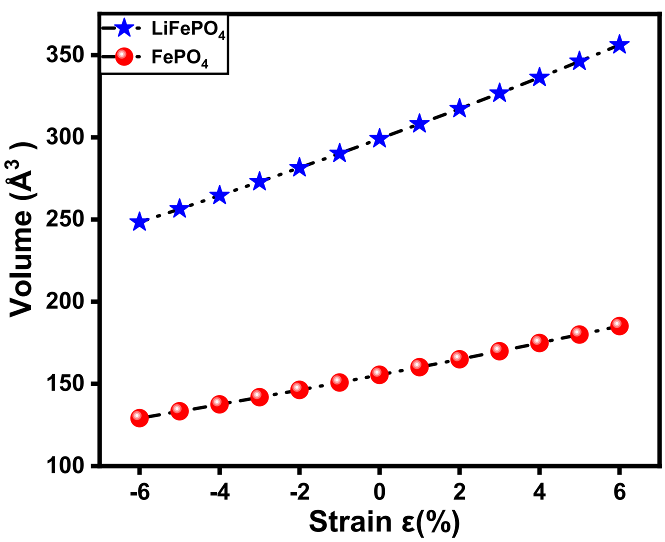

Fig. 2. Variation in volume of $LiFePO_4$ and $FePO_4$ as a function of applied strains.

Fig. 2 shows that the volume of $LiFePO_4$ is 299.1 Å^3, It is in good agreement with the results obtained in another study, which are 294.718 Å^3 [10], while that of $FePO_4$ is 155.45 Å^3. Under tensile strains of +6 %, these values increase to 356.22 Å^3 and 185.15 Å^3, respectively. This increase indicates that the atoms in both systems move farther apart under tension, creating additional space between them. This phenomenon suggests a structural reorganization within the materials, which could have significant implications for their thermodynamic and electronic properties, as well as for the diffusion kinetics of Li^+ during battery charging and discharging. On the other hand, under compressive strains of −6 %, the volume of $LiFePO_4$ and $FePO_4$ shows an opposite behavior. Specifically, the volume decreases linearly, reaching values of 248.42 Å^3 for $LiFePO_4$ and 129.12 Å^3 for $FePO_4$, respectively. This contraction indicates that the atoms in both systems move closer together when subjected to compressive forces [17]. This volume reduction is significant, as it can affect the stability and mechanical properties of the materials, as well as their performance in practical applications.

3.3. Energy of absorption

As shown in the section dedicated to the variation of volume under triaxial tensile and compressive strains, these strains lead to a significant variation in volume. This variation can be explained by changes in the total energies of the $LiFePO_4$ and $FePO_4$ systems, which directly influence the energy of absorption of Li^+ ions during the charge and discharge phases of batteries under triaxial strains. Furthermore, when a strain is applied, the energy of the system changes in response to the reorganization of atoms and the modification of interatomic distances. These energy changes provide insights into the stability and interactions within both the $LiFePO_4$ and $FePO_4$ systems, thus improving our understanding of their behavior under various strain conditions. The energy of absorption is defined as the difference between the total energy of the $LiFePO_4$ system and the energies of $FePO_4$ and Li^+ ions [22,65,76]. The equation for this calculation is as follows:

$$\Delta E = E_{tot}(LiFePO_4) - E_{tot}(FePO_4) - E_{tot}(Li) \quad (4)$$

The variation in the absorption energy under triaxial strains applied to $LiFePO_4$ and $FePO_4$ is illustrated in Fig. 3.

Fig. 3-a shows that the absorption energy of Li^+ ions varies with changes in volume induced by the applied strains. For the free $LiFePO_4$ and $FePO_4$ systems, the absorption energy is measured at −3.92 eV. In contrast, Kaifu Zhong and al, based their study on the GGA-PBE approach and found that the absorption energy for the free system is −2.18 eV [69]. This difference in values can be attributed to the methodology used and the inherent approximations in each approach. As shown in Fig. 3-a, the absorption energy varies with the applied stress. It changes from its initial value of −3.92 eV for the undeformed $LiFePO_4$ to −3.32 eV under a tensile stress of +6 % and increases to −3.08 eV under a compressive stress of −6 %. And this shows that the variation in volume resulting from changes in tensile and compressive stress leads to an increase in absorption energy. This correlation can be explained by the fact that an increase or decrease in volume creates

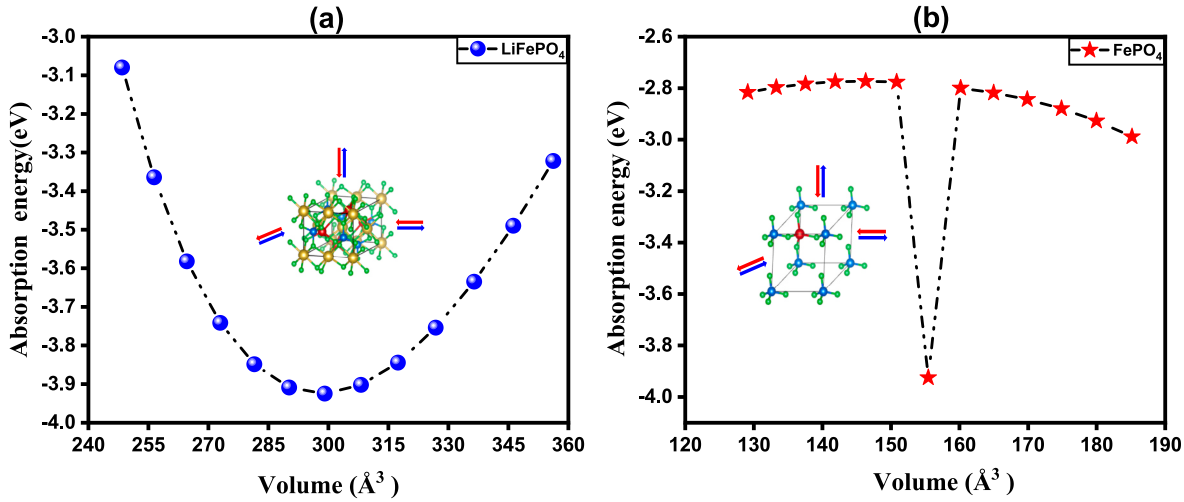

Fig. 3. Variation in the absorption energy of Li^+ ions as a function of volume under applied strains on $LiFePO_4$ (a) and $FePO_4$ (b).

space between the atoms in the unit cell of $LiFePO_4$, greater or smaller than in the undeformed state. This can lead to a rearrangement of the atoms in the unit cell. As a result, the absorption of Li^+ ions during this rearrangement would be more difficult. This leads to increased agitation of the valence electrons, making the propagation of Li^+ ions more difficult. As a result, variations in absorption energy are directly related to structural changes and atomic interactions within the system. On the other hand, as shown in Fig. 3-b, the tensile or compressive strains applied to the $FePO_4$ system show that the absorption energy increases, particularly under the first tensile +1 % or compressive strain of −1 %. The absorption energy increases from −3.92 eV for the undeformed $FePO_4$ to −2.8 eV under the +1 % tensile strain, and to −2.78 eV under the first −1 % compressive strain. This significant increase in absorption energy can be explained by the fact that the strains lead to the creation of stronger bonding forces within the $FePO_4$ system, making it more thermodynamically stable. After the initial tensile (+1 %) and compressive (−1 %) strains, the absorption energy undergoes a slight decrease, which can be explained by the reduction in the agitation of the valence electrons or by the contribution of atomic orbitals. It should be noted that the effect of the strains on the contribution of orbitals to the bonding will be explained in more detail later, particularly in Fig. 8. This slight decrease in absorption energy for the $FePO_4$ system reaches a value of −2.99 eV when the tensile strain is +6 %. In the case of the maximum compressive strain of −6 %, the absorption energy stabilizes at −2.82 eV. This clearly shows that the first strain applied to $FePO_4$ leads to a significant reduction in the absorption energy of lithium ions in the cathode. In addition to the initial interpretation, this decrease can also be explained by modifications in the crystalline structure of the material, which influence the interactions between the lithium ions and the absorbing $FePO_4$ system.

3.4. Open circuit voltage (OCV)

In general, the open circuit voltage (OCV) is the primary factor determining the reliability of cathodes used in batteries [22,65,76]. When the OCV is between 2.5 V and 4.5 V, the material used for the cathode is considered viable. However, if the OCV exceeds 4.5 V, the risk of explosion becomes more likely, and if the voltage drops below 2.5 V, irreversible reactions may affect the battery's performance [65]. Therefore, optimization of the material is necessary, This optimization may involve modifications to the chemical composition, crystalline structure, or manufacturing process to enhance the performance and stability of the cathode, ensuring better efficiency and a longer lifespan for the battery [42,49]. To calculate the OCV, we will apply the following equation (5):

$$V_{ocv} = \frac{\Delta E}{e} \tag{5}$$

With ΔE representing the absorption energy and *e* being the absolute value of the electron charge, the variation of the OCV under triaxial tensile and compressive strains is schematized in Fig. 4.

Fig. 4 shows that the open circuit voltage (OCV) for the undeformed $LiFePO_4$ and $FePO_4$ systems is 3.92 V. This value falls within the operating voltage range (2.5–4.5 V) for battery cathodes [22,86]. In other studies, the open circuit voltage value of $LiFePO_4$ is 3.6728 V and 4.62 V [90,91]. This difference in open circuit voltage values is due to the calculation methods and cathode optimization techniques. This result is significant because it ensures the reliability of the method chosen in our study. Additionally, it reveals a similarity with the operational requirements of lithium-ion batteries $LiFePO_4$, which is crucial for ensuring good cathode efficiency. In contrast, Fig. 4-a demonstrates that the application of increasing strains to the $LiFePO_4$ system alters the initial OCV value, while still keeping it within the battery operating range (2.5–4.5 V). For instance, under a maximum tensile strain of +6 %, the OCV value drops to 3.32 V, while it reaches 3.08 V under a maximum compressive strain of −6 %. This result could contribute to research on improving lithium-ion batteries, making them capable of operating across a wide range of temperatures. On the other hand, Fig. 4-b shows that the OCV drops significantly with the first applied strain on the $FePO_4$ system of ±1 % amplitude. At this strain level, the OCV decreases to 2.79 V under a +1 % tensile strain and 2.77 V under a −1 % compressive strain. This drop in OCV is linked to the decrease in the desorption energy of Li^+ ions, a phenomenon we discussed earlier. When strains are applied to the $FePO_4$ system, this induces a modification in the structure and interactions within the cathode, leading to a reduction in the lithium ions' ability to desorb efficiently, resulting in a drop in OCV. However, the OCV remains within the operating range for cathodes, typically between 2.5 V and 4.5 V. This indicates that, despite the drop in open circuit voltage due to the applied strains, the battery still maintains sufficient operational capacity to function effectively. After this initial drop in OCV, the application of triaxial tensile/compressive strain leads to a slight increase in the OCV, which eventually reaches 2.98 V under a maximum tensile strain of +6 %, and 2.82 V under a maximum compressive strain of −6 %. This variation in OCV opens new perspectives for future research, offering the potential to better control the cathode voltage by adjusting the applied strains, whether tensile or compressive.

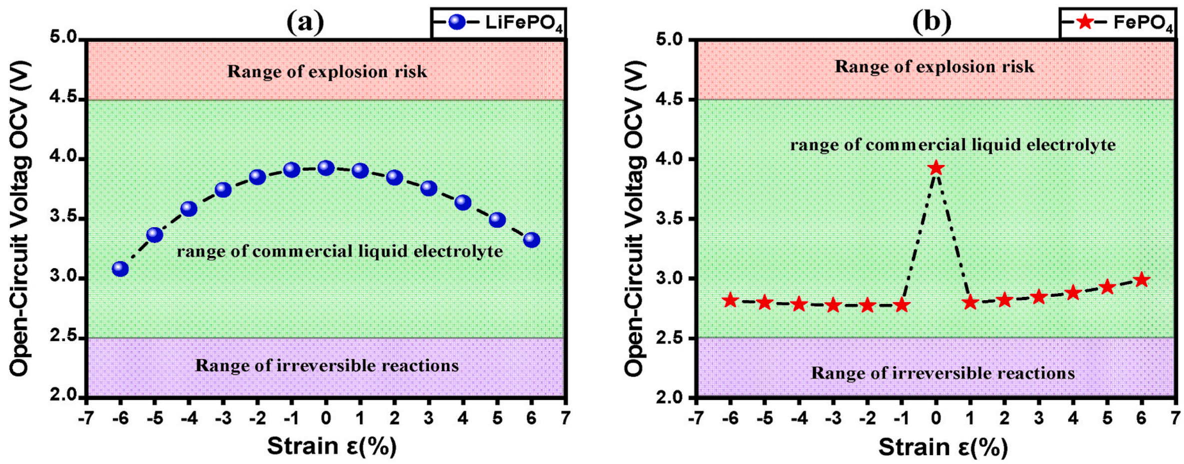

Fig. 4. Variation of the open circuit voltage (OCV) as a function of the triaxial strains applied to $LiFePO_4$ (a) and $FePO_4$ (b).

3.5. Energy density

Energy density is generally defined as the amount of energy that a material can store. In our case, it refers to the amount of energy a lithium battery can store per unit of mass. This energy is directly influenced by the variation in the open-circuit voltage (OCV) generated by the cathode. Understanding this energy helps in optimizing lithium-based cathodes under different triaxial tensile and compressive stress. As demonstrated by Aled D. Roberts and al [92], energy density can be expressed as follows:

$$E_d = \frac{n \times F \times V_{ocv}}{3600 \times M_c} \tag{6}$$

With n being the number of moles of electrons transferred during the electrochemical reaction, F the Faraday constant, V_{OCV} the open-circuit voltage of the cathode, and *Mc* the molar mass of the cathode material. The results of the energy density optimization under the application of triaxial tensile/compressive stress on the two systems $LiFePO_4$ and $FePO_4$ are presented in Fig. 5.

Fig. 5-a shows that the energy density decreases in both cases, under tensile or compressive stress. For the undeformed system, the energy density is 666.83 Wh/kg with an open circuit voltage (OCV) of 3.92 V. This value is close to the one found by Mourad Rkhis and al [65], which is 572.923 Wh/kg with an OCV of 3.37 V. When the $LiFePO_4$ system is subjected to a maximum tensile strain of +6 %, the energy density becomes 564.42 Wh/kg, with an OCV of 3.32 V. Conversely, in the case of maximum compression of −6 %, the energy density is 523.28 Wh/kg with an OCV of 3.08 V. For the $FePO_4$ system, under tensile/compressive stress (Fig. 5-b), the energy density inevitably drops as a result of the first applied strain of ±1 %. For a tensile strain of +1 %, the energy density reaches 475.63 Wh/kg, while for a compressive strain of −1 %, it drops to 471.7 Wh/kg, with the corresponding voltages of 2.8 V and 2.78 V, respectively. The energy density then shows a nearly constant increase, ultimately reaching 507.71 Wh/kg under a maximum tensile strain of +6 %, with the corresponding voltage at this strain equal to 2.99 V. In contrast, under a maximum compressive strain of −6 %, the energy density is 478.46 Wh/kg, with the corresponding voltage at 2.82 V. This variation in energy density is directly related to the changes in OCV, which also vary depending on the applied stress. Thus, it can be concluded that triaxial stress provide a way to control the variation in OCV and, consequently, manage the variation in energy density, which can influence the performance of $LiFePO_4$ lithium-ion batteries. Indeed, tensile or compressive strains do not increase energy density. As shown in equation (6), energy density is related to the open circuit voltage (OCV). In our case, deformation is not beneficial, but it opens up perspectives for future research. For example, if a voltage higher than 4.5 V is reached, strains should be applied to reduce it and bring it within the 2.5–4.5 V range (the commercialization range for batteries). This decrease in (OCV) would be followed by a reduction in energy density but would help avoid the risk of explosion.

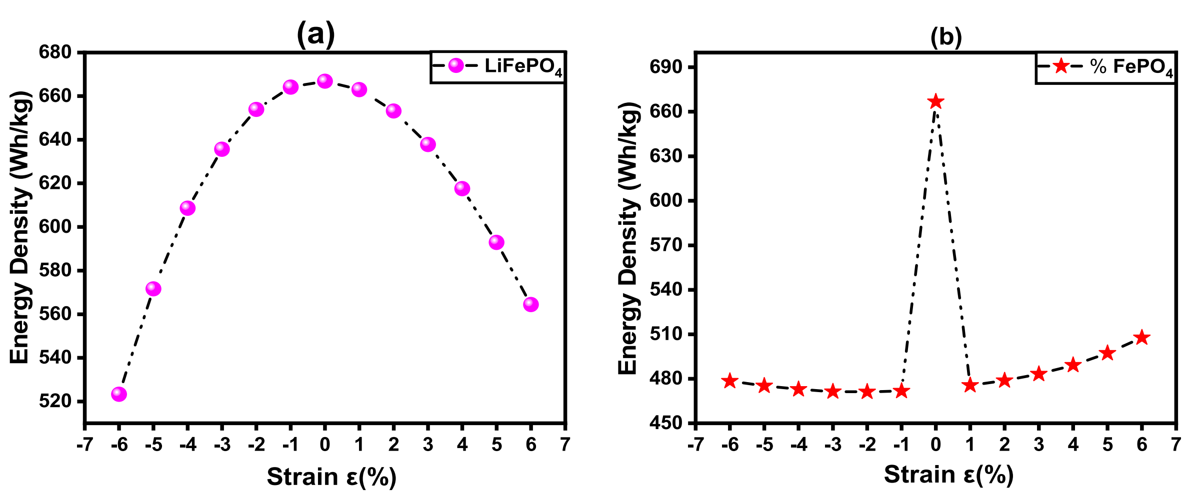

Fig. 5. *Variation of energy density under triaxial stress applied to $LiFePO_4$ (a) and $FePO_4$ (b).*

3.6. Variation in the distance between (P–O) and (Fe–O)

When the $LiFePO_4$ and $FePO_4$ systems are subjected to strain, the interatomic distance can be influenced by the migration of ions within these two systems, from one site to another. Thus, understanding the variations in the distance between atoms in a given system under strain can provide insights into the changes in open-circuit voltage (OCV) as well as the alterations in charge density, a topic that will be further explored in this work [65]. To achieve this goal, we calculate the variations in the distances between the phosphorus and oxygen atoms on one hand, and between the iron and oxygen atoms on the other hand, in both the $LiFePO_4$ and $FePO_4$ systems under triaxial tensile and compressive strains. The results of these distances are illustrated in Fig. 6.

As shown in Fig. 6, when triaxial tensile and compressive strains are applied, the distances between the P–O and Fe–O atoms undergo changes, but these variations are much more pronounced in the case of the $LiFePO_4$ system subjected to tensile and compressive deformations compared to $FePO_4$. Specifically, when applying strains to $LiFePO_4$, the distance between P–O increases from 1.519 Å to 1.534 Å under a maximum tensile strain of +6 % and decreases to 1.491 Å under a maximum compressive strain of −6 %. On the other hand, the distance between Fe–O changes from 2.083 Å for the undeformed $LiFePO_4$ system to 2.229 Å under a maximum tensile strain of +6 % and decreases to 1.956 Å under a maximum compressive strain of −6 %. This significant variation is attributed to the ionic interactions between the ions in the $LiFePO_4$ system. On the other hand, when the $FePO_4$ system is subjected to tensile or compressive strains, the variations in the distance between the P–O atoms remain nearly constant, changing only by 0.06 %–1 % compared to the undeformed $FePO_4$ system. Meanwhile, the variation in the distance between Fe–O under the applied triaxial tensile and compressive strains on $FePO_4$ ranges from 0.1 % to 2.3 % relative to the undeformed $FePO_4$ system. This small variation in the P–O and Fe–O distances when strains are applied to $FePO_4$ reflects the high stability of the $FePO_4$ system.

3.7. Charge density

In the field of batteries, understanding the electronic charge density generally allows us to determine how much charge a material can store, as well as the success of the electrochemical reactions facilitated by the cathode [93]. Indeed, a low distribution of charges within the electrodes can reduce the speed of oxidation and reduction reactions, which may lead to a shorter battery life, and vice versa. Furthermore, the electronic charge density helps to identify the types of bonding in the studied system and analyze charge transfer under applied constraints, whether tensile or compressive. With this in mind, we have determined the electronic charge density and represented it in the [100], [010], and [001] directions to better understand the electronic behavior of the $LiFePO_4$ system under triaxial constraints [68,84]. The results obtained are illustrated in Fig. 7.

Before presenting the results of the electronic charge density obtained in this research, it is essential to understand the types of bonds formed in the $LiFePO_4$ system. First, lithium (Li), being an alkali metal, easily loses its valence electron to form the Li^+ ion. On the other hand, the phosphate ion PO_4^{3-} is negatively charged and forms an ionic bond with the Li^+ ion, ensuring an electrostatic interaction between these two ions [74]. Next, in the phosphate ion PO_4^{3-}, phosphorus (P) forms covalent bonds with the four oxygen atoms, allowing the formation of a stable tetrahedral structure. As for iron (Fe), it is typically found in the Fe^{2+} oxidation state, where it is surrounded by six oxygen atoms, forming an octahedral FeO_6 complex [94]. In this complex, the electron sharing between iron Fe^{2+} and oxygen O^{2-} is more polar, as oxygen is more electronegative than iron [95]. Therefore, the interactions between Li^+, Fe^{2+}, and PO_4^{3-} ions are responsible for the formation of the crystal lattice and contribute to maintaining the cohesion of the $LiFePO_4$ solid.

As shown in Fig. 7, the representation of the electronic charge density of $LiFePO_4$, both under strain and in free conditions, along the three crystallographic directions [100], [010], and [001], reveals that the electron density is much higher around the PO_4^{3-} ion, as oxygen is the most electronegative element among those that make up $LiFePO_4$. This density decreases in relation to the bonds formed between the PO_4^{3-} phosphate group and the Li^+ and Fe^{2+} ions, but it remains significant in the case of the interaction between PO_4^{3-} and Li^+, as the ionic bond leads to a relatively significant electron transfer. In contrast, in the case of the bonds between PO_4^{3-} and Fe^{2+}, the electron sharing is lower, as the bond is polar, with iron having a lower electronegativity than oxygen. On the other hand, the electron density can be influenced by the applied strains. For example, when a maximum tensile strain of +6 % is applied, we observe that the electron sharing between the PO_4^{3-}, Li^+, and Fe^{2+} ions starts to decrease. In contrast, when a maximum compressive strain of −6 % is applied, this electron sharing increases. This is particularly evident from the dotted lines, which illustrate the electron sharing behavior. These lines converge under compression and diverge under tension. This variation can be explained by the atoms coming closer together under compression, while they move farther apart under tension. Ultimately, we can conclude that the applied strains not only

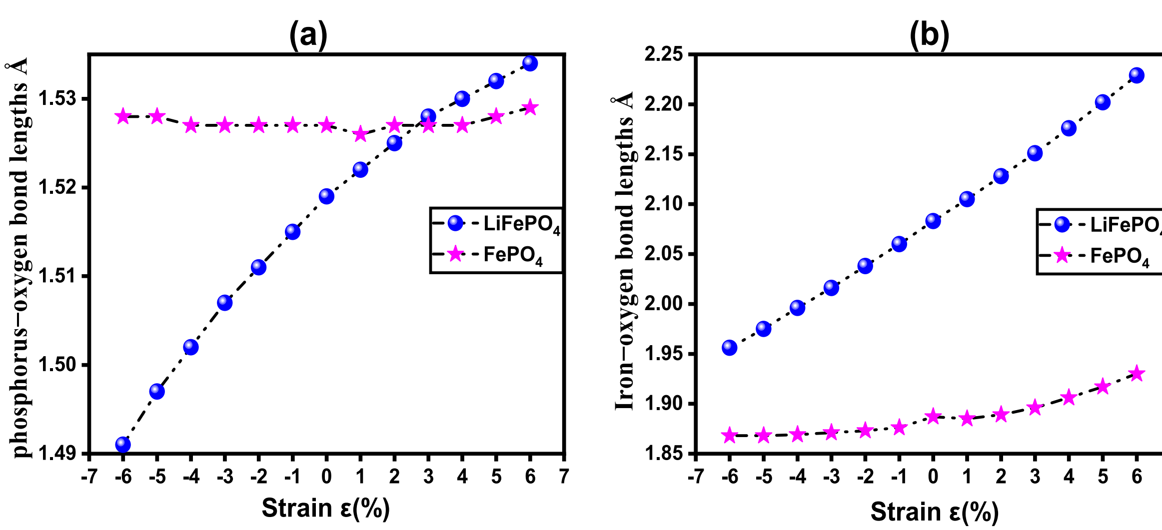

Fig. 6. Variation of the interatomic distance in the $LiFePO_4$ and $FePO_4$ systems under triaxial strain between P–O (a), and Fe–O (b).

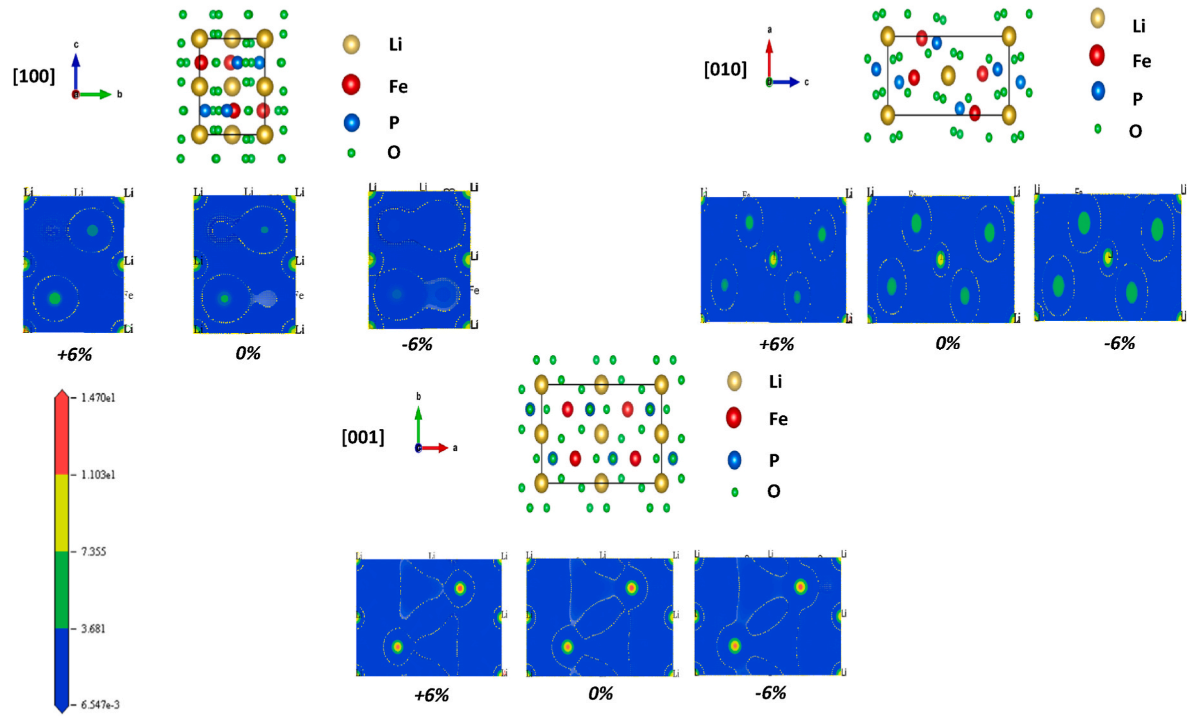

Fig. 7. Distributions of electronic charge density in $LiFePO_4$ under maximum tensile/compressive strain in the [100], [010], and [001] directions.

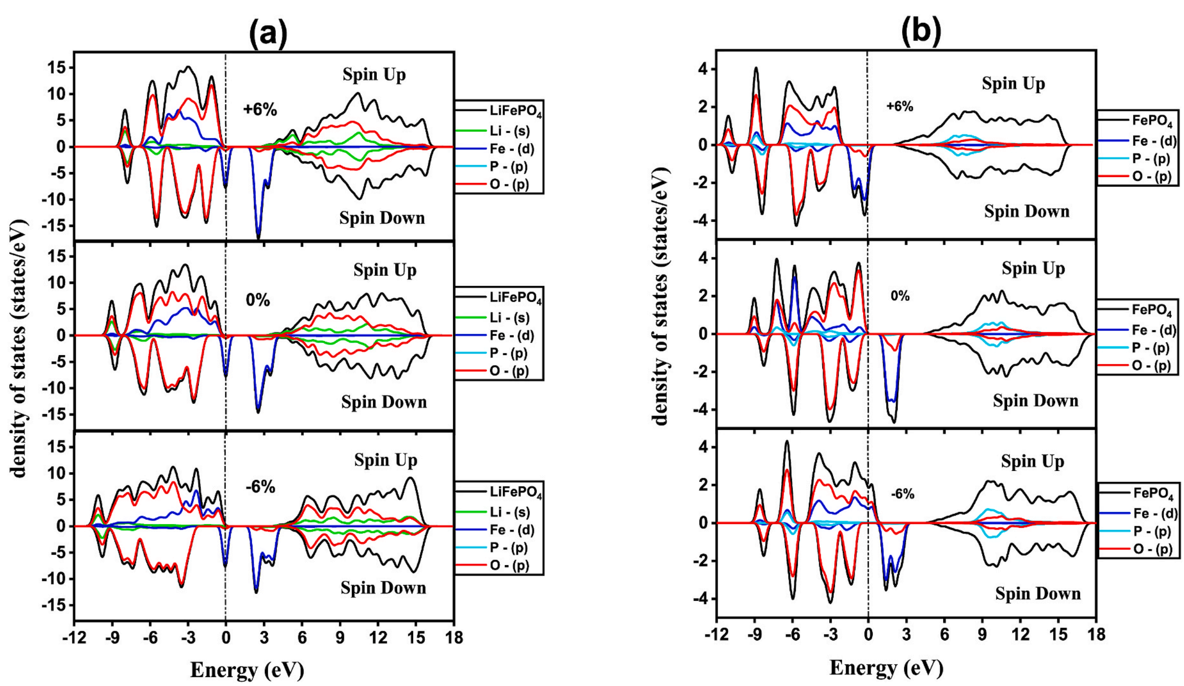

Fig. 8. Total Electronic Density of States (TDOS) and Partial Density of States (PDOS) for the free and triaxially strained systems, $LiFePO_4$ (a) and $FePO_4$ (b).

improve the open-circuit voltage (OCV), but also promote redox reactions, which can further optimize the charge and discharge cycles of the $LiFePO_4$ battery. This will enable future research to gain insights into the durability of catalysts based on charge distribution and could also guide these studies in finding solutions to the durability problem.

3.8. Electronic properties

As we previously determined, the electron density varies depending on the bonds formed between the ions in the lithium states of $LiFePO_4$. In this context, and to gain a better understanding of the electronic states of the lithium system $LiFePO_4$ and the iron-free $FePO_4$ system, we calculated the total density of states (TDOS) as well as the partial density of states (PDOS) for both spin-up and spin-down states [32,86]. The results are illustrated in Fig. 8, where the dashed line indicates the Fermi level, set to 0.

Fig. 8-a shows that the unstrained $LiFePO_4$ system exhibits semiconductor behavior with a bandgap of 2.256 eV, which is in good

agreement with other results found in the literature: 2.24 eV [96] and 2.69 eV [65]. This small variation is attributed to the calculation method used. This energy gap can vary depending on the applied stress, but with a small amplitude. Additionally, the density of states also changes under the influence of these stress. For example, in the case of spin-up states, the conduction band is primarily populated by oxygen (p) states and iron (d) states, while in the case of spin-down states, the conduction band is mainly filled with oxygen (p) states, with a minor contribution from phosphorus (p) states and lithium (s) states. The valence band, within the energy range of 2.256 eV–5 eV, is populated by iron (d) states for the spin-down case, while a lack of states is observed for the spin-up case. In the energy range of 5 eV–15 eV, both for spin-up and spin-down, the band is generally filled with oxygen (p) states and lithium (s) states. Moreover, the peaks in the total density of states (TDOS) undergo significant changes: they increase under tension and decrease under compression. The large peak in the conduction band for the spin-up case increases from 13.45 (states/eV) for the undeformed $LiFePO_4$ system to 15.05 (states/eV) under a +6 % tensile strain and decreases to 11.43 (states/eV) under a −6 % compressive strain. Similarly, the large peak in this band for the spin-down case increases from −13 (states/eV) for the undeformed $LiFePO_4$ system to −14.04 (states/eV) under +6 % tensile strain and decreases to −11.71 (states/eV) under −6 % compressive strain. The peaks in the total density of states (TDOS) follow the same trends: they increase under tension and decrease under compression. More specifically, the large peak in absolute value in the valence band for both spin-up and spin-down is 8.27 (states/eV), and it increases to 10.39 (states/eV) under +6 % tensile strain, while it decreases to 6.87 (states/eV) under −6 % compressive strain.

Fig. 8-b shows that the undeformed system is characterized as a semiconductor with a gap of 1.831 eV, which is in good agreement with other previously published results: 1.46 eV [ref] and 1.37 eV [ref]. However, this characteristic does not hold under applied strains. For instance, applying compressive strain turns the material metallic, with a gap of 0 eV. This behavior is due to the strong bonding between ions, which move closer together under compression in $FePO_4$. In contrast, under tensile strain, the gap increases and reaches 2.09 eV, as a result of the ions moving further apart. Furthermore, the valence bandwidth elongates under tension and narrows under compression. Specifically, the valence bandwidth is [−9.48; 0] eV for the undeformed $FePO_4$ system, and becomes [−11.66; 0] eV when subjected to +6 % tensile strain, and [−9.14; 0] eV under −6 % compressive strain. The same phenomenon has been reported in other applications using triaxial and biaxial strains to enhance thermodynamic properties for hydrogen storage. The contribution of states in the $FePO_4$ system to the valence band is generally dominated by iron (d) states and oxygen (p) states for spin-up cases. Conversely, for spin-down cases, the contribution is entirely from oxygen (p) states, with a small contribution from phosphorus (p) and iron (d) states. For the valence band, the contribution of phosphorus (p) states becomes more prominent, whether for spin-up or spin-down cases, with a minor contribution from iron (d) states and oxygen (p) states.

3.9. Band gap

To fully understand the effect of triaxial strains on the bandgap, which can also impact charge transfer during cathode operation, we will study the bandgap under the effect of triaxial tensile/compressive strains applied to both lithiumated $LiFePO_4$ and de-lithiated $FePO_4$ systems [65]. The results obtained are shown in Fig. 9.

As shown in Fig. 9-a, when the $LiFePO_4$ system is subjected to compressive strain, the bandgap decreases significantly, from 2.265 eV for the undeformed system to 2.089 eV for the system under a maximum compression of −6 %. This substantial decrease can be attributed to the ionic interactions between the Li^+, Fe^{2+}, and PO_4^{3-} ions, which move closer together under the applied strain, thereby facilitating electron sharing. In contrast, under tensile strain, the bandgap decreases but to a lesser extent, reaching 2.233 eV under a +6 % tensile strain. This can be interpreted as the result of weaker interactions between the ions in the case of tension.

Fig. 9-b shows a significant change in the case of compression, where the bandgap drops from 1.831 eV for the undeformed $FePO_4$ system to 0 eV under the first compression of −1 %, then experiences a slight increase, eventually reaching 0.355 eV under a compression of −6 %. This sharp decrease followed by a slight increase can be interpreted as the compression pushing the ions to form a more stable structure, leading to a minimal modification in their arrangement after this transformation. In contrast, under tensile strain, the bandgap increases, reaching up to 2.09 eV under a +6 % tensile strain. This increase is due to the reduced interaction between the ions.

4. Conclusion

In this work, triaxial stress have been applied to optimize and control the open-circuit voltage (OCV) as well as the energy density under these stress for the lithium-based $LiFePO_4$ battery cathode. The study also focuses on the thermodynamic, electrochemical, electronic, and structural properties based on the generalized gradient approximation (GGA). The results show that.

- ✓ The triaxial stress applied to $LiFePO_4$ allow the open-circuit voltage (OCV) to vary between 3.08 V and 3.92 V, while for $FePO_4$, the OCV

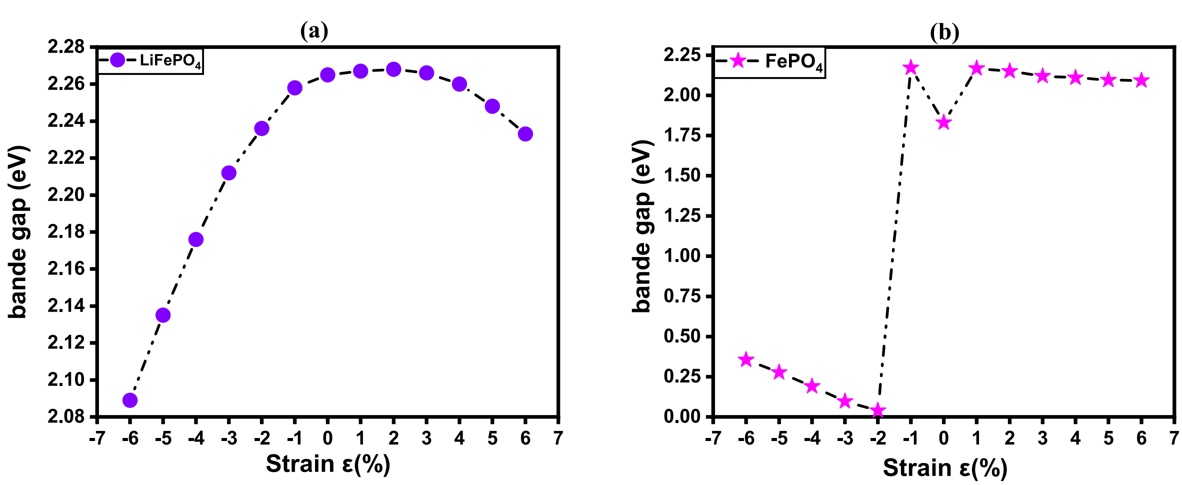

Fig. 9. Variation of the bandgap under triaxial strain for $LiFePO_4$ (a) and $FePO_4$ (b) systems.

varies between 2.81 V and 3.92 V, all within the voltage range of commercial batteries (2.5 V–4.5 V).

✓ The triaxial stress are capable of varying the energy density between 523.28 and 666.83 Wh/kg when applied to $LiFePO_4$, and between 478.46 and 666.83 Wh/kg when applied to $FePO_4$.

✓ The absorption energy of lithium ions (Li^+) varies between −2.81 eV and −3.92 eV depending on the stress applied to $LiFePO_4$ or $FePO_4$.

✓ The charge density is significantly higher when compression stress are applied compared to tensile stress on $LiFePO_4$, which helps improve the performance of the cathode.

CRediT authorship contribution statement

Abdelmajid Assila: Writing – review & editing, Writing – original draft, Visualization, Validation, Supervision, Resources, Methodology, Formal analysis, Data curation. **Ikram Belkoufa:** Writing – review & editing, Software, Resources. **Seddiq Sebbahi:** Writing – review & editing, Visualization, Resources. **Amine Alaoui-Belghiti:** Writing – review & editing, Supervision, Software, Investigation, Data curation. **Said laasri:** Writing – review & editing, Writing – original draft, Validation, Supervision, Software, Methodology, Data curation. **El-kebir Hlil:** Writing – review & editing, Writing – original draft, Visualization, Validation, Resources, Methodology, Investigation. **Mouhaydine Tlemçani:** Visualization, Validation, Software, Resources, Methodology, Formal analysis. **Abdelowahed Hajjaji:** Writing – review & editing, Visualization, Validation, Supervision, Resources, Investigation, Formal analysis, Data curation.

Declaration of competing interest

The authors declare that they have no known competing financial interests or personal relationships that could have appeared to influence the work reported in this paper.

References

[1] Lehmann-Hasemeyer S, Prettner K, Tscheuschner P. The scientific revolution and its implications for long-run economic development. World Dev 2023;168:106262. https://doi.org/10.1016/j.worlddev.2023.106262.

[2] Elsayed AH, Billah M, Goodell JW, Hadhri S. Examining connections between the fourth industrial revolution and energy markets. Energy Econ 2024;133:107476. https://doi.org/10.1016/j.eneco.2024.107476.

[3] Groumpos PP. A critical historical and scientific overview of all industrial revolutions. IFAC-PapersOnLine 2021;54:464–71. https://doi.org/10.1016/j.ifacol.2021.10.492.

[4] Miah MT, Fariha JN, Kafy A-A, Islam R, Biswas N, Duti BM, et al. Exploring the nexus between land cover change dynamics and spatial heterogeneity of demographic trajectories in rapidly growing ecosystems of south Asian cities. Ecol Indic 2024;158:111299. https://doi.org/10.1016/j.ecolind.2023.111299.

[5] Gunasegaran J, Teh Y-Y, Lim C-K, Ng S-F. Review on prevalence, risk factors, and research advancements on the use of medical gloves concerning hand dermatitis among health care workers. Saf Work Health 2024;15:129–38. https://doi.org/10.1016/j.shaw.2024.02.005.

[6] Rayed MdE, Islam SMS, Niha SI, Jim JR, Kabir MM, Mridha MF. Deep learning for medical image segmentation: state-of-the-art advancements and challenges. Inform Med Unlocked 2024;47:101504. https://doi.org/10.1016/j.imu.2024.101504.

[7] Tang R, Wang S, Shan K, Cheung H. Optimal control strategy of central air-conditioning systems of buildings at morning start period for enhanced energy efficiency and peak demand limiting. Energy 2018;151:771–81. https://doi.org/10.1016/j.energy.2018.03.032.

[8] Zou C, Ma F, Pan S, Zhao Q, Fu G, Zhang G, et al. Global energy transition revolution and the connotation and pathway of the green and intelligent energy system. Petrol Explor Dev 2023;50:722–40. https://doi.org/10.1016/S1876-3804(23)60423-9.

[9] Yang J, Yu Y, Ma T, Zhang C, Wang Q. Evolution of energy and metal demand driven by industrial revolutions and its trend analysis. Chin J Popul Resour Environ 2021;19:256–64. https://doi.org/10.1016/j.cjpre.2021.12.028.

[10] Zaki NHM, Ahmad SI, Sazman FN, Badrudin FW, Abdullah ALA, Taib MFM, et al. The influence of Cl doping on the structural, electronic properties and Li-ion migration of LiFePO4: a DFT study. Comput Theor Chem 2023;1221:114029. https://doi.org/10.1016/j.comptc.2023.114029.

[11] Liu J, Liang K, He J, Li J, Huang X, Zhang X, et al. Functionalized porous conductive carbon layer improves the low-temperature performance of LiFePO4 cathode material for lithium-ion batteries. Carbon 2024;229:119483. https://doi.org/10.1016/j.carbon.2024.119483.

[12] Zhang Z, Hu J, Hu Y, Wang H, Hu H. Lithium fluorosulfonate-induced low-resistance interphase boosting low-temperature performance of commercial graphite/LiFePO4 pouch batteries. J Colloid Interface Sci 2024;669:305–13. https://doi.org/10.1016/j.jcis.2024.05.009.

[13] Scarpati G, Frasci E, Di Ilio G, Jannelli E. A comprehensive review on metal hydrides-based hydrogen storage systems for mobile applications. J Energy Storage 2024;102:113934. https://doi.org/10.1016/j.est.2024.113934.

[14] Nanda J, Martha SK, Porter WD, Wang H, Dudney NJ, Radin MD, et al. Thermophysical properties of LiFePO4 cathodes with carbonized pitch coatings and organic binders: experiments and first-principles modeling. J Power Sources 2014;251:8–13. https://doi.org/10.1016/j.jpowsour.2013.11.022.

[15] Rostami H, Valio J, Suominen P, Tynjälä P, Lassi U. Advancements in cathode technology, recycling strategies, and market dynamics: a comprehensive review of sodium ion batteries. Chem Eng J 2024;495:153471. https://doi.org/10.1016/j.cej.2024.153471.

[16] Xu G, Zhong K, Yang Y, Zhang J-M, Huang Z. Insight into delithiation process on the $LiFePO_4$ (010) surface from a novel viewpoint of the work function. Solid State Ionics 2019;338:25–30. https://doi.org/10.1016/j.ssi.2019.05.009.

[17] Assila A, Rkhis M, Alaoui-Belghiti A, Laasri S, Hlil EK, Boughaleb Y, et al. Feeling the strain: enhancing the thermodynamics characteristics of magnesium nickel hydride Mg2NiH4 for hydrogen storage applications through strain engineering. Int J Hydrogen Energy 2024;67:651–7. https://doi.org/10.1016/j.ijhydene.2024.04.159.

[18] Assila A, Rkhis M, Sebbahi S, Alaoui Belghiti A, Laasri S, Hlil EK, et al. Improvement of the thermodynamic properties of lithium borohydride LiBH4 by mechanical treatment for hydrogen storage applications: a DFT investigation. Int J Hydrogen Energy 2024;51:72–8. https://doi.org/10.1016/j.ijhydene.2023.10.317.

[19] He K, Zhang Z-Y, Zhang F-S. A green process for phosphorus recovery from spent LiFePO4 batteries by transformation of delithiated LiFePO4 crystal into NaFeS2. J Hazard Mater 2020;395:122614. https://doi.org/10.1016/j.jhazmat.2020.122614.

[20] Alaoui-Belghiti A, Assila A, Belkoufa I, Rkhis M, Laasri S, Tlemçani M, et al. Strain engineering for optimized hydrogen storage: enhancing ionic conductivity and achieving near-room-temperature desorption in Mg_2NiH_4. Int J Hydrogen Energy 2024;92:1069–77. https://doi.org/10.1016/j.ijhydene.2024.10.292.

[21] Xu J, Chen G. Effects of doping on the electronic properties of LiFePO4: a first-principles investigation. Phys B Condens Matter 2010;405:803–7. https://doi.org/10.1016/j.physb.2009.05.035.

[22] Hariti N, Assila A, Rkhis M, Laasri S, Belhora F, El Idrissi M, et al. Density functional theory calculations applied to olivine-like $NaMnPO_4$ with transition metal substitutions for energy storage applications. Eur Phys J Appl Phys 2024;99:20. https://doi.org/10.1051/epjap/2024240037.

[23] Zhang J, Huang YN, Peng P, Mao C, Shao YM, Zhou DW. First-principles study on the dehydrogenation properties and mechanism of Al-doped Mg2NiH4. Int J Hydrogen Energy 2011;36:5375–82. https://doi.org/10.1016/j.ijhydene.2011.02.002.

[24] Liu X, Zhang Y, Meng Y, Xiao M, Kang T, Gao H, et al. Preparation and electrochemical properties of Co doped core-shell cathode material on a lithium iron phosphate surface. J Alloys Compd 2022;923:166326. https://doi.org/10.1016/j.jallcom.2022.166326.

[25] Shi Z, Wang T, Shi Z, Cui S, Zhang Z, Liu W, et al. Synergetic effects of Fe N C and LiFePO4 in modified separator on improved adsorption and catalytic conversion reaction of soluble LiPSs for Lithium-sulfur batteries. Chem Eng J 2023;457:141264. https://doi.org/10.1016/j.cej.2022.141264.

[26] Li J, Fan W, Qin W, Ma C, Yan L, Guo Y, et al. The regeneration process of FePO4 in electrochemical lithium extraction: the role of alkali ions. Chem Eng J 2024;493:152476. https://doi.org/10.1016/j.cej.2024.152476.

[27] Zeng Z, Lei H, Li J, Wang B, Lei S, Ji X, et al. Regenerated spent LiFePO4 with tailored residual copper-atoms towards improved energy-storage capacity and reversibility. Chem Eng J 2024;499:155616. https://doi.org/10.1016/j.cej.2024.155616.

[28] Tang Z, Xie Z, Cai Q, Xia Z, Chen Q, Liang W, et al. Unlocking superior safety, rate capability, and low-temperature performances in LiFePO4 power batteries. Energy Storage Mater 2024;67:103309. https://doi.org/10.1016/j.ensm.2024.103309.

[29] Awasthi S, Moharana S, Kumar V, Wang N, Chmanehpour E, Sharma AD, et al. Progress in doping and crystal deformation for polyanions cathode based lithium-ion batteries. Nano Mater Sci 2024;S2589965124000047. https://doi.org/10.1016/j.nanoms.2024.01.004.

[30] Wheatcroft L, Özkaya D, Cookson J, Inkson BJ. Towards in-situ TEM for Li-ion battery research. Energy Proc 2018;151:163–7. https://doi.org/10.1016/j.egypro.2018.09.042.

[31] Mao Z-Y, Sun Y-P, Scott K. Evaluation of apparent lithium-ion diffusion coefficients in FePO4/LiFePO4 cathode material particles from linear non-equilibrium thermodynamics and principle of electroneutrality. J Electroanal Chem 2016;766:107–19. https://doi.org/10.1016/j.jelechem.2016.01.018.

[32] Rkhis M, Alaoui-Belghiti A, Laasri S, Touhtouh S, Hajjaji A, Hlil EK, et al. First principle investigation on hydrogen solid storage in Zr1-xNbxNiH3 ($x = 0$ and 0.1). Int J Hydrogen Energy 2019;44:23188–95. https://doi.org/10.1016/j.ijhydene.2019.07.017.

[33] Belkoufa I, Misski B, Alaoui-Belghiti A, Mouyane M, Houivet D, Laasri S, et al. Role of Mg, Ca, and Mo in NaBH4 systems for hydrogen storage applications: Ab initio study. Comput Mater Sci 2024;242:113090. https://doi.org/10.1016/j.commatsci.2024.113090.

[34] Assila A, Belkoufa I, Sebbahi S, Alaoui-Belghiti A, Hlil E, Tlemçani M, et al. The role of Al substitution in Na3AlH6 hydrides: structural and thermodynamic insights

for hydrogen storage technologies. J Power Sources 2025;634:236502. https://doi.org/10.1016/j.jpowsour.2025.236502.

[35] Belkoufa I, Assila A, Alaoui-Belghiti A, Laasri S, Hlil EK, Hajjaji A. Strain matters: enhancing the hydrogenation properties of Mg_2CoH_5 through multiaxial approaches. Int J Hydrogen Energy 2025;105:1114–22. https://doi.org/10.1016/j.ijhydene.2025.01.353.

[36] Klebanoff LE, Keller JO. 5 Years of hydrogen storage research in the U.S. DOE metal hydride center of excellence (MHCoE). Int J Hydrogen Energy 2013;38:4533–76. https://doi.org/10.1016/j.ijhydene.2013.01.051.

[37] Belkoufa I, Misski B, Alaoui-Belghiti A, Moslah C, Mouyane M, Houivet D, et al. Improved thermodynamic properties of (Sc, V, Ti, Fe, Mn, Co, and Ni) doped NaBH4 for hydrogen storage: first-principal calculation. Int J Hydrogen Energy 2024;68:481–90. https://doi.org/10.1016/j.ijhydene.2024.04.155.

[38] Ignatova AA, Kozlov AV, Shestakov AF, Chernyak AV, Yarmolenko OV, Troshin PA. Insight in the degradation of polyquinone-based cathode material in lithium-organic battery under cycling. Mendeleev Commun 2017;27:524–6. https://doi.org/10.1016/j.mencom.2017.09.032.

[39] Guan X, Li G, Li C, Ren R. Synthesis of porous nano/micro structured LiFePO4/C cathode materials for lithium-ion batteries by spray-drying method. Trans Nonferrous Metals Soc China 2017;27:141–7. https://doi.org/10.1016/S1003-6326(17)60016-5.

[40] Shen C, Lin W, Hu H, Yang P, Wang L. The electronic and geometric structure modifications of LiFePO4 with vanadium doping to achieve ultrafast discharging capability: the experimental and theoretical investigations. J Alloys Compd 2023;936:168035. https://doi.org/10.1016/j.jallcom.2022.168035.

[41] Pan X, Zhuang S, Sun Y, Sun G, Ren Y, Jiang S, et al. Restraining formation of Fe-Li anti-site defects via in-situ surface construction on single-crystal LiFePO4 cathode for extending fast charging lifespan. J Alloys Compd 2023;968:172257. https://doi.org/10.1016/j.jallcom.2023.172257.

[42] Il'ina EA. Effect of heat treatment on the interface resistance between LiFePO4 and Li7La3Zr2O12. Solid State Ionics 2024;414:116638. https://doi.org/10.1016/j.ssi.2024.116638.

[43] Liu J, Lin X, Han T, Li X, Gu C, Li J. A novel litchi-like LiFePO4 sphere/reduced graphene oxide composite Li-ion battery cathode with high capacity, good rate-performance and low-temperature property. Appl Surf Sci 2018;459:233–41. https://doi.org/10.1016/j.apsusc.2018.07.199.

[44] Shi S, Zhang H, Ke X, Ouyang C, Lei M, Chen L. First-principles study of lattice dynamics of LiFePO4. Phys Lett 2009;373:4096–100. https://doi.org/10.1016/j.physleta.2009.09.014.

[45] Yu S-Y, Zhang C-G, Liang J, Wang X. Design of Ti, Zr-doped butadiene nanobuilding blocks for hydrogen storage materials: a density functional theory investigation. J Comput Theor Nanosci 2016;13:399–403. https://doi.org/10.1166/jctn.2016.4819.

[46] Huang C-Y, Kuo T-R, Yougbaré S, Lin L-Y. Design of LiFePO4 and porous carbon composites with excellent High-Rate charging performance for Lithium-Ion secondary battery. J Colloid Interface Sci 2022;607:1457–65. https://doi.org/10.1016/j.jcis.2021.09.118.

[47] Lin W, Yang P, Zhou K, Wang L, Shen C. Indium doping: an effective route to optimize the electrochemical performance of LiFePO4 cathode material. Solid State Ionics 2023;403:116322. https://doi.org/10.1016/j.ssi.2023.116322.

[48] Sumita M, Tanaka Y, Ikeda M, Ohno T. Theoretical insight into charging process in a Li3PO4 (100)/LiFePO4 (010) coherent interface system. Solid State Ionics 2016;285:59–65. https://doi.org/10.1016/j.ssi.2015.09.029.

[49] Gao L, Xu Z, Zhang S, Xu J, Tang K. Enhanced electrochemical properties of LiFePO 4 cathode materials by Co and Zr multi-doping. Solid State Ionics 2017;305:52–6. https://doi.org/10.1016/j.ssi.2017.04.021.

[50] Chen H, Yang K, Shao J, Liu Y, Zhang M, Wei B, et al. Explosion dynamics for thermal runaway gases of 314 Ah LiFePO4 lithium-ion batteries triggered by overheating and overcharging. Process Saf Environ Prot 2024;192:1238–48. https://doi.org/10.1016/j.psep.2024.10.111.

[51] Zhao X, Wang X, Guo J, Gu Z, Cao J, Yang J, et al. Dynamic Li^+ capture through ligand-chain interaction for the regeneration of depleted $LiFePO_4$ cathode. Adv Mater 2024;36:2308927. https://doi.org/10.1002/adma.202308927.

[52] Li C, Zhang J, Sun J, Zhao Y, Zhou J, Wang H, et al. Electronic effect tuned ion-dipole interactions for low-temperature electrolyte design of LiFePO4-based lithium-ion batteries. J Energy Storage 2024;102:114207. https://doi.org/10.1016/j.est.2024.114207.

[53] Li X, Yu L, Cui Y, Li A, Shao H, Shao Z, et al. Enhanced properties of LiFePO4/C cathode materials co-doped with V and F ions via high-temperature ball milling route. Int J Hydrogen Energy 2019;44:27204–13. https://doi.org/10.1016/j.ijhydene.2019.08.187.

[54] Li X, Shao Z, Liu K, Zhao Q, Liu G, Xu B. A facile ultrasound assisted high temperature ball milling synthesis of LiFePO4/graphene with enhanced electrochemical performance. Int J Hydrogen Energy 2018;43:18773–82. https://doi.org/10.1016/j.ijhydene.2018.08.061.

[55] Jiang ZY, Li HB, Qu ZG, Zhang JF. Recent progress in lithium-ion battery thermal management for a wide range of temperature and abuse conditions. Int J Hydrogen Energy 2022;47:9428–59. https://doi.org/10.1016/j.ijhydene.2022.01.008.

[56] Göktepe H, Şahan H, Patat Ş. Effect of silver and carbon double coating on the electrochemical performance of LiFePO4 cathode material for lithium ion batteries. Int J Hydrogen Energy 2016;41:9774–9. https://doi.org/10.1016/j.ijhydene.2016.03.074.

[57] Li Z, You Y, Zhu Z, Wang L, Ou S, Xu J, et al. Surface iron concentration gradient: a strategy to suppress Mn3+ Jahn-Teller effect in lithium manganese iron phosphate. Appl Surf Sci 2025;682:161689. https://doi.org/10.1016/j.apsusc.2024.161689.

[58] Jeong SY, Lee S, Lee H, Roh K-M, Lee C-W, Jeong I, et al. Thermal characteristics of LiMnxFe1-xPO4 (x = 0, 0.6) cathode materials for safe lithium-ion batteries. J Power Sources 2025;626:235755. https://doi.org/10.1016/j.jpowsour.2024.235755.

[59] Liu Q, Wen D, Yu X, Jiang H. Effect of Na-Si co-doping on the performance of LiFePO4. J Electroanal Chem 2023;950:117891. https://doi.org/10.1016/j.jelechem.2023.117891.

[60] Chang Q, Yao G, Pan F, Chen D, Wang W, Yan W. Investigation on interfacial interaction and the origin of Fe3+ in LiFePO4/C. Electrochim Acta 2013;108:211–8. https://doi.org/10.1016/j.electacta.2013.06.058.

[61] Nakayama M, Yamada S, Jalem R, Kasuga T. Density functional studies of olivine-type LiFePO4 and NaFePO4 as positive electrode materials for rechargeable lithium and sodium ion batteries. Solid State Ionics 2016;286:40–4. https://doi.org/10.1016/j.ssi.2015.12.019.

[62] Xiong Z-C, Xie Y, Yi T-F, Yu H, Zhu Y-R, Zeng Y-Y. Effect of lithium extraction on the stabilities, electrochemical properties, and bonding characteristics of LiFePO4 cathode materials: a first-principles investigation. Ceram Int 2014;40:2655–61. https://doi.org/10.1016/j.ceramint.2013.10.059.

[63] Lin J, Sun Y-H, Lin X. Metal-organic framework-derived LiFePO4 cathode encapsulated in O,F-codoped carbon matrix towards superior lithium storage. Nano Energy 2022;91:106655. https://doi.org/10.1016/j.nanoen.2021.106655.

[64] Meng Y, Li Y, Xia J, Hu Q, Ke X, Ren G, et al. F-doped LiFePO4@N/B/F-doped carbon as high performance cathode materials for Li-ion batteries. Appl Surf Sci 2019;476:761–8. https://doi.org/10.1016/j.apsusc.2019.01.139.

[65] Rkhis M, Nabil N. The art of strain engineering: fine-tuning the electrochemical performance of olivine Ferrophosphate LiFePO4 as cathode materials for Li-ion batteries. J Energy Storage 2024;97:112815. https://doi.org/10.1016/j.est.2024.112815.

[66] Shim T-Y, Yoo Y-W, Lee J-K, Kim Y-J, Yoon J-R, Kim K-N, et al. Enhanced C-rate capability and long-term cycling behavior of LiFePO4/C-BaTiO3 composite cathode. J Energy Storage 2024;90:111915. https://doi.org/10.1016/j.est.2024.111915.

[67] Yao C, Wang F, Chen J, Yin M. First-principles study of the structural and electronic properties of LiFePO4 by graphene and N-doped graphene modification. Comput Theor Chem 2022;1217:113897. https://doi.org/10.1016/j.comptc.2022.113897.

[68] Zhou F, Kang K, Maxisch T, Ceder G, Morgan D. The electronic structure and band gap of LiFePO4 and LiMnPO4. Solid State Commun 2004;132:181–6. https://doi.org/10.1016/j.ssc.2004.07.055.

[69] Zhong K, Cai X, Wang M. The mechanism of easier desorption of Fe atoms on the (1 0 0) surface of LiFePO4 and FePO4. Chem Phys 2023;570:111891. https://doi.org/10.1016/j.chemphys.2023.111891.

[70] Ren X, Li Y, He Z, Xi X, Shen X. In-situ growth of LiFePO4 with interconnected pores supported on carbon nanotubes via tavorite-olivine phase transition. Ceram Int 2023;49:40131–9. https://doi.org/10.1016/j.ceramint.2023.09.344.

[71] Johnson ID, Lübke M, Wu OY, Makwana NM, Smales GJ, Islam HU, et al. Pilot-scale continuous synthesis of a vanadium-doped LiFePO4/C nanocomposite high-rate cathodes for lithium-ion batteries. J Power Sources 2016;302:410–8. https://doi.org/10.1016/j.jpowsour.2015.10.068.

[72] Shellikeri A, Yturriaga S, Zheng JS, Cao W, Hagen M, Read JA, et al. Hybrid lithium-ion capacitor with LiFePO4/AC composite cathode – long term cycle life study, rate effect and charge sharing analysis. J Power Sources 2018;392:285–95. https://doi.org/10.1016/j.jpowsour.2018.05.002.

[73] Yusuf A, Sai Avvaru V, De La Vega J, Zhang M, Garcia Molleja J, Wang D-Y. Unveiling the structure, chemistry, and formation mechanism of an in-situ phosphazene flame retardant-derived interphase layer in LiFePO4 cathode. Chem Eng J 2023;455:140678. https://doi.org/10.1016/j.cej.2022.140678.

[74] Zhang Y, Alarco JA, Nerkar JY, Best AS, Snook GA, Talbot PC. Nanoscale characteristics of practical LiFePO4 materials - effects on electrical, magnetic and electrochemical properties. Mater Char 2020;162:110171. https://doi.org/10.1016/j.matchar.2020.110171.

[75] An Q, Liu Q, Wang S, Liu L, Wang H, Sun Y, et al. Oxygen vacancies with localized electrons direct a functionalized separator toward dendrite-free and high loading LiFePO4 for lithium metal batteries. J Energy Chem 2022;75:38–45. https://doi.org/10.1016/j.jechem.2022.08.006.

[76] Wang S, Wang F. Effect of Mn, N co-doped LiFePO4 on electrochemical and mechanical properties: a DFT study. J Mol Graph Model 2023;125:108604. https://doi.org/10.1016/j.jmgm.2023.108604.

[77] Nayak C, Bhasin V, Halankar KK, Banerjee S, Bute A, Jha SN, et al. Operando X ray absorption spectroscopy elucidating the de-lithiation/lithiation mechanism of Mn and Ni co-doped LiFePO4 cathodes. J Electroanal Chem 2024;969:118536. https://doi.org/10.1016/j.jelechem.2024.118536.

[78] Rutter MJ. C2x: a tool for visualisation and input preparation for Castep and other electronic structure codes. Comput Phys Commun 2018;225:174–9. https://doi.org/10.1016/j.cpc.2017.12.008.

[79] Pacheco-Kato JC, Del Campo JM, Gázquez JL, Trickey SB, Vela A. A PW91-like exchange with a simple analytical form. Chem Phys Lett 2016;651:268–73. https://doi.org/10.1016/j.cplett.2016.03.028.

[80] Hasnip PJ, Pickard CJ. Electronic energy minimisation with ultrasoft pseudopotentials. Comput Phys Commun 2006;174:24–9. https://doi.org/10.1016/j.cpc.2005.07.011.

[81] He J-N, Kumaresan T, Yu T, Fang W, Natarajan S. Numerical implementation and comparison study on simulating thermo-elastic fracture using adaptive phase-field method combined with BFGS algorithm and AM algorithm. Theor Appl Fract Mech 2024;133:104650. https://doi.org/10.1016/j.tafmec.2024.104650.

[82] Babaie–Kafaki S, Aminifard Z, Ghafoori S. Nonmonotone diagonally scaled limited-memory BFGS methods with application to compressive sensing based on a penalty

model. Appl Numer Math 2022;181:618–29. https://doi.org/10.1016/j.apnum.2022.07.008.

[83] Tair M, Baaddi M, Omari LH, Maouhoubi A, Drissi S, Farkad O, et al. Triaxial strain effects on hydrogen storage capacity of $KMgH_3$: a computational study. Inorg Chem Commun 2024;169:112974. https://doi.org/10.1016/j.inoche.2024.112974.

[84] Benzidi H, Lakhal M, Benyoussef A, Hamedoun M, Loulidi M, El kenz A, et al. First principle study of strain effect on structural and dehydrogenation properties of complex hydride $LiBH_4$. Int J Hydrogen Energy 2017;42:19481–6. https://doi.org/10.1016/j.ijhydene.2017.06.068.

[85] Rkhis M, Laasri S, Touhtouh S, Hlil EK, Bououdina M, Ahuja R, et al. Engineering the hydrogen storage properties of the perovskite hydride $ZrNiH_3$ by uniaxial/biaxial strain. Int J Hydrogen Energy 2022;47:3022–32. https://doi.org/10.1016/j.ijhydene.2021.10.237.

[86] Alfaruqi MH, Kim S, Park S, Lee S, Lee J, Hwang J-Y, et al. Density functional theory investigation of mixed transition metals in olivine and tavorite cathode materials for Li-ion batteries. ACS Appl Mater Interfaces 2020;12:16376–86. https://doi.org/10.1021/acsami.9b23367.

[87] Wang SZ, Zhang G, Gao JL, Wang J, Wang YY, Nan CJ, et al. First-principles study on $LiFePO_4$ materials for lithium-ion battery. Proceedings of the international workshop on materials, chemistry and engineering. Xiamen. China: SCITEPRESS - Science and Technology Publications; 2018. p. 133–8. https://doi.org/10.5220/0007435601330138.

[88] Sundarayya Y, Vijeth H, Nagaraju D, Kumara Swamy KC, Sunandana CS. Isovalent substitution of vanadium in $LiFePO_4$: evolution of monoclinic α-$Li_3Fe_2(PO_4)_3$ phase. Inorg Chem Commun 2023;150:110530. https://doi.org/10.1016/j.inoche.2023.110530.

[89] Zhang D, Wang J, Dong K, Hao A. First principles investigation on the elastic and electronic properties of Mn, Co, Nb, Mo doped $LiFePO_4$. Comput Mater Sci 2018;155:410–5. https://doi.org/10.1016/j.commatsci.2018.09.010.

[90] Yang Z, Guo Y, Zhang X, Tang W, Li B, Feng Y. Valence electron structure and properties of $LiTPO_4$/C (T = Mn, Fe, Co, Ni) lithium-ion batteries. J Energy Storage 2024;91:111963. https://doi.org/10.1016/j.est.2024.111963.

[91] Kanungo S, Bhattacharjee A, Bahadursha N, Ghosh A. Comparative analysis of $LiMPO_4$ (M = Fe, Co, Cr, Mn, V) as cathode materials for lithium-ion battery applications—a first-principle-based theoretical approach. Nanomaterials 2022;12:3266. https://doi.org/10.3390/nano12193266.

[92] Roberts AD, Li X, Zhang H. Porous carbon spheres and monoliths: morphology control, pore size tuning and their applications as Li-ion battery anode materials. Chem Soc Rev 2014;43:4341–56. https://doi.org/10.1039/C4CS00071D.

[93] Shi S, Liu L, Ouyang C, Wang D, Wang Z, Chen L, et al. Enhancement of electronic conductivity of $LiFePO_4$ by Cr doping and its identification by first-principles calculations. Phys Rev B 2003;68:195108. https://doi.org/10.1103/PhysRevB.68.195108.

[94] Chen Z, Wang F, Li T, Wang S, Yao C, Wu H. First-principles study of $LiFePO_4$ modified by graphene and defective graphene oxide. J Mol Graph Model 2024;129:108731. https://doi.org/10.1016/j.jmgm.2024.108731.

[95] Moore EK, Ostroverkhova A, Hummer D, Morrison S, Peralta Y, Spielman SJ. The influence of oxygen and electronegativity on iron mineral chemistry throughout Earth's history. Precambr Res 2023;386:106960. https://doi.org/10.1016/j.precamres.2022.106960.

[96] Lethole NL, Ngoepe PE, Chauke HR. First-principles study: effect of lithium and sodium intercalation in transition metal phosphates, MPO_4 (M: Mn, Fe, Co). Comput Condens Matter 2020;22:e00437. https://doi.org/10.1016/j.cocom.2019.e00437.